Striped-phase germanene confirmed by photoemission final-state effect

Ting-Yu Chen [1,*] Chin-Hsuan Chen,[1,*] David Mikolas,[1] Santosh Chiniwar [1] Angus Huang,[1] Chung-Huang Lin,[1] Cheng-Maw Cheng [2] Fumio Komori,[3] Iwao Matsuda,[3] Chung-Yu Mou [1,4] Horng-Tay Jeng,[1,4,6] Woei Wu Pai,[5] and S.-J. Tang [1,2,4,‡]

[1]*Center for Quantum Science and Department of Physics, National Tsing Hua University, Hsinchu 300, Taiwan*
[2]*National Synchrotron Radiation Research Center (NSRRC), Hsinchu 30076, Taiwan*
[3]*Institute for Solid State Physics, The University of Tokyo, Kashiwa, Chiba 277-8581, Japan*
[4]*Institute of Physics, Academia Sinica, Taipei 11529, Taiwan*
[5]*Center for Condensed Matter Sciences and Department of Physics, National Taiwan University, Taipei 106, Taiwan*
[6]*Physics Division, National Center for Theoretical Sciences, Taipei 10617, Taiwan*

(Received 15 August 2024; accepted 1 November 2024; published 22 November 2024)

The formation of germanene on Ag(111) has been extensively studied and confirmed. However, the nature of the transition stage between the initial Ag_2Ge alloy phase at 1/3 monolayer (ML) and the final quasifreestanding phase germanene phase at coverage $\geqslant$1 ML still remains elusive. Using angle-resolved photoemission spectroscopy, scanning-tunneling microscopy (STM), and low-energy electron diffraction, we confirm the existence of striped-phase (SP) germanene in the transition stage. Along the armchair direction of SP, the period of higher-order coincidence corresponds to $11a_{\mathrm{AC}} = 31a_{\mathrm{Ag(111)}}$, which accommodates four stripes on the bridge sites of the underlying Ag(111) lattice, as manifested in STM topography. On the electronic-structure side, the splitlike surface band of Ag_2Ge centered at the surface zone boundary $\bar{M}_{\mathrm{Ag(111)}}$ evidently evolves to a steep, V-shaped interfacial-state band, characteristic of SP germanene. Moreover, an anomalous broad Ag bulk-state band was observed to fully develop upon formation of SP germanene. The bulk-state band originates from the direct transition to the final-state bands of originally d character at ∼22–23 eV above the Fermi level. Because of the strong hybridization between germanene π and Ag d orbitals, the unoccupied Ag bulk final-state d bands near the interface take on p_z character, inducing the direct transition from the Ag bulk occupied p_z-valence band, following the selection rule for the photoemission cross section. A germanene identity of SP is thus confirmed. Our result indicates a very important missing segment of the evolution from the initial surface alloy phase to the final Xene layer, which is the coexistence of both in a common stripe lattice during a continuous transition.

DOI: 10.1103/PhysRevResearch.6.043190

I. INTRODUCTION

The discovery of graphene has triggered a lot of interest in growing a monatomic layer with a honeycomb lattice, the analogs of which belong to the family of two-dimensional (2D) Xenes [1] such as silicene [2,3], germanene [4–7], stanene [8,9], plumbene [10,11], borophene [12,13], bismuthene [14], gallenene [15], phosphorene [16], arsenene [17], antimonene [18], selenene [19], and tellurene [20]. Among them, silicene and germanene are more graphenelike not only because of composite elements being in the same group, that is, group IV, but also the covalent-bond nature of bulk silicon and germanium crystals. Such directional bonding can provide more flexibility to bear tensile strain, and therefore a large variety of honeycomb forms are likely to exist. On the other hand, unlike sp^2 trigonal-planar bonds in graphene, silicene and germanene adopt sp^3 tetrahedral bonds [21] so their growth on a substrate is more subject to the narrow-condition window that corresponds to a special form in a metastable state. Compared to silicene, germanene has been more widely seen to form on several substrates such as Ag(111) [4–7], Al(111) [22], GePt [23], MoS_2 [24], etc. Lin *et al.* [5] deposited Ge atoms onto Ag(111) at an elevated temperature of 150° C and demonstrated two different phases of germanene forming at different coverage, namely, the striped phase (SP) and the quasifreestanding (QP) phase at 0.74 and 1.08 monolayer (ML), through consistent results for lattice and electronic structures determined from scanning-tunneling microscopy (STM), low-energy electron diffraction (LEED), and angle-resolved photoemission spectroscopy (ARPES). SP germanene undergoes large tensile strain along the stripe direction [5,7] to match the underlying Ag(111)-$\sqrt{3}\times\sqrt{3}R30^\circ$ lattice but partially relaxes in the armchair (AC) direction to reach a balance with the interfacial strain. Upon further Ge deposition, SP germanene completely relaxes its tensile strain to become QP, with a lattice constant of 3.91 Å, a bit smaller than the calculated 4.06 Å for freestanding germanene. The

*These authors contributed equally to this work.
‡Contact author: sjtang@phys.nthu.edu.tw

σ band centered at the zone boundary $\bar{K}_{QP}$ was observed [5], indicating less interfacial interaction with Ag(111). A list of distinct energy band structures characterizing Ag_2Ge, SP, and QP germanene are shown in Fig. S1 of the Supplemental Material [25]. Chen *et al.* [7] showed that addition of extra Pb instead of Ge atoms to SP could not only lead to the transition, but also evidently improved the lattice and electronic quality of QP germanene due to the interaction with the side-by-side Pb layer. Although SP structure is also observed in other Xene such as borophene [26] and beryllene [27], the existence of SP germanene has not been universally accepted. Using STM to measure the advance of Ag step edges, Zhang *et al.* [28] determined the Ag concentration when Ge was deposited onto Ag(111) in the 380–430 K temperature range and concluded that for 1/3 ML, the substitutional Ag_2Ge alloy formed a striped phase. Up to a coverage of 0.6 ML, a disordered hexagonal structure is obtained, which is also interpreted as an alloy with a larger proportion of Ge atoms. They further proposed the $c(31 \times \sqrt{3})$ lattice model [29] for the striped Ag_2Ge alloy, which was deduced from the measurement of surface x-ray diffraction and backed up by density-functional theory (DFT) calculation. Kesper *et al.* [4] employed low-energy electron diffraction (LEED) and x-ray photoelectron spectroscopy, together with x-ray photoelectron diffraction to investigate the structural evolution of germanene on Ag(111) and claimed that above 1/3 ML, the Ag_2Ge $\sqrt{3} \times \sqrt{3}R30^\circ$ surface alloy turns into a more complex superstructure of $\text{Rec}(\sqrt{3} \times 17)$ due to a tensile strain of the uppermost layer of the surface alloy and at 0.6 ML, a mixed phase—the transition phase before the formation of QP germanene—takes place as a superposition of the coexisting surface alloy and the $\text{Rec}\{c(\sqrt{3} \times 7)\}$ reconstruction of the germanene formation. The conclusions of the preceding studies, however, cannot rule out the possibility that Ag_2Ge surface alloy and germanene intermix in the common stripe lattice; the former diminishes and the latter grows as the coverage increases from 1/3 to 0. 74 ML. The best way to clarify the picture is by carefully investigating the evolution of distinct electronic structures, especially valence bands, characterizing Ag_2Ge surface alloy and SP germanene, respectively, in this coverage range. In this paper, we first apply a model to simulate the atomic arrangement of SP germanene on Ag(111), which matches the corresponding STM-resolved honeycomb lattice very well with the lattice constant verified by precise LEED analysis. We then systematically investigate the electronic-structure evolution during the transition to SP germanene. Finally, the anomalous direct-transition band upon SP formation was measured and carefully analyzed to further confirm the existence of SP germanene.

II. EXPERIMENTAL PROCEDURES AND CALCULATION METHODS

A. Germanene growth

The germanene samples were prepared on a Ag(111) single crystal, with Ge evaporated from an effusion cell kept at 965° C and with the substrate kept at 150° C. The deposition rate is approximately 0.01–0.02 ML per minute. Here 1 ML refers to the number density of atoms of the top Ag(111) layer. The silver crystal was cleaned by repeated sputter-anneal cycles and its cleanness was verified by sharp LEED diffraction spots and by direct STM imaging. Although the range of conditions for germanene formation has not been explored fully, a slower Ge deposition rate along with a moderately heated substrate facilitates better germanene growth, likely due to reduced random nucleation and enhanced Ge adatom mobility [5].

B. STM measurement

All STM/STS scans were performed on a commercial omicron low temperature scanning tunneling microscopy (RHK SPM-1000 control system) in ultrahigh vacuum at liquid nitrogen temperature, 77 K, and with homemade chemical-etched tungsten tips.

C. Photoemission measurement

Core-level and valence-band photoemission spectra were measured with a Scienta R4000 (R3000) energy analyzer and *p*-polarized synchrotron radiation from the beamline 21B1-U9 (08A1-LSGM) at the National Synchrotron Radiation Research Center in Taiwan. The energy and angular resolutions were 10 meV and 0.3°, and 50 meV and 0.3°, respectively.

D. LEED simulation

Throughout all the LEED simulation results shown in this paper, we use a lattice constant of 2.889 Å [30] for the bulk Ag(111) crystal surface. The muffin-tin internal energy was adjusted in each simulation to produce all of the kinematically allowed spots which correspond to those observed in the LEED images.

E. DFT calculation

The *ab initio* simulations were performed by the Vienna *ab initio* simulation package (VASP) code [31–33] based on density-functional theory (DFT). The exchange-correlation functional used the Perdew-Burke-Ernzerhof (PBE) type of generalized gradient approximation (GGA) [31].

For simulation of bulk silver electronic properties, a $24 \times 24 \times 24$ Monkhorst-Pack k mesh and an energy cutoff 400 eV were used in the self-consistent field calculations. The total energies are converged to within 10^{-4} eV. To simulate the surface-state electronic states, the 3×4 supercell SP germanene monolayer cover at a 2×8, 6-ML Ag (111) slab are considered. The size of the vacuum region used is 23 Å. The $2 \times 8 \times 1$ Monkhorst-Pack k mesh in the 2D Brillouin zone and a cutoff energy of 250 eV are used in the self-consistent field calculations. The total energies are converged the same as bulk silver calculation. To compare with the experiment results, we unfold the band structures of the SP/Ag (111) supercells to the first Brillouin zone of Ag (111) unit cell by using the BANDUP package [34,35].

III. RESULTS AND DISCUSSION

Figures 1(a)–1(h) show a series of LEED patterns, taken at 50 eV, for the step-by-step deposition of Ge atoms onto Ag(111) at the temperature of 150° C. Before deposition

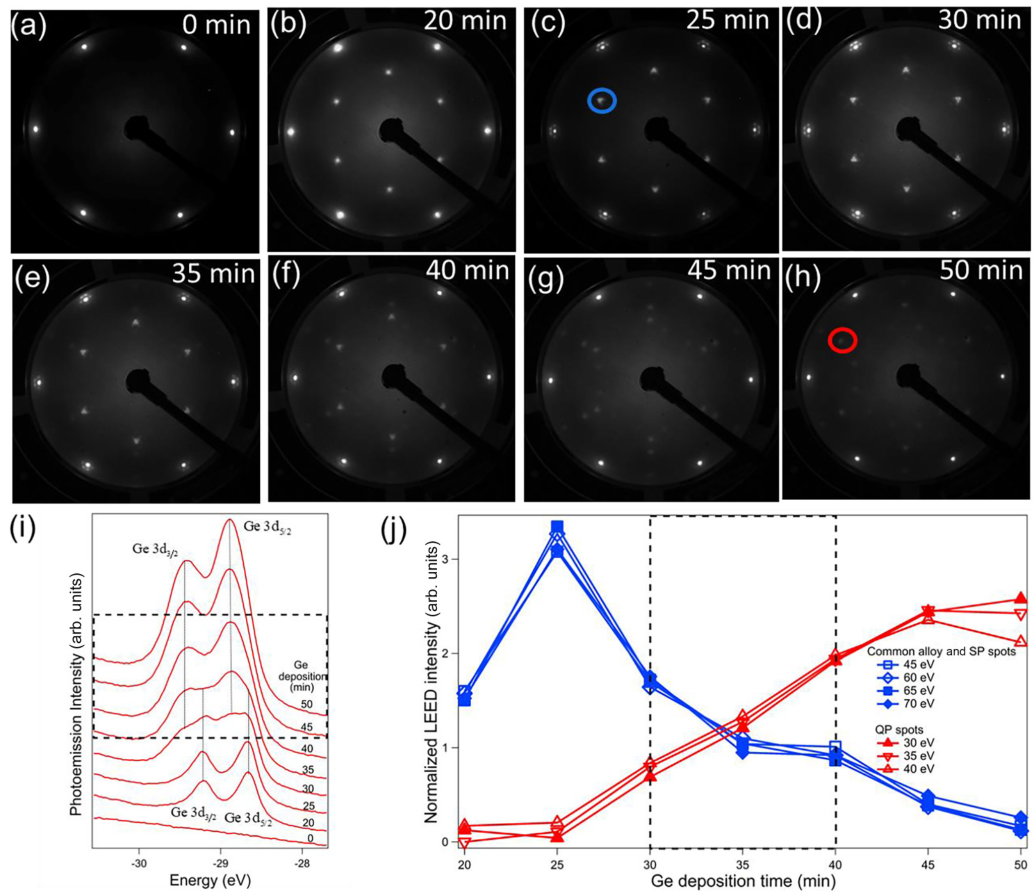

FIG. 1. Step-by-step time dependence of Ge deposition onto Ag(111) at 150° C for (a)–(h) LEED patterns taken at 50 eV, (i) Ge $3d$ core-level spectra taken at 80 eV, and (j) the LEED intensities of QP single scattering (red) and Ag(111)-$\sqrt{3} \times \sqrt{3}R30^\circ$ spots (blue), respectively. The electron energies employed correspond to LEED spots which are more distinguishable.

begins ($t = 0$ min), the LEED pattern of Fig. 1(a) shows the 1×1 spots of Ag(111). At 20 min, the Ag(111)-$\sqrt{3} \times \sqrt{3}R30^\circ$ spots appear at the $(\frac{1}{3}\ \frac{1}{3})$ positions, indicating the formation of Ag_2Ge surface alloy [36]. At 25 min, satellitelike spots emerge around the (10) and $(\frac{1}{3}\ \frac{1}{3})$ positions. This was ascribed to the development of striped lattice structures of Ag_2Ge surface alloy in three rotational domains spaced at 120° from each other [37]. When deposition time surpasses 35 min, one can see the new spots developing outside of $(\frac{1}{3}\ \frac{1}{3})$. They are single scattering spots of QP germanene. At 50 min, all the spots related to striped structures are nearly gone and QP-related spots remain. The corresponding Ge $3d$ core-level spectra concurrently measured for the same time points are stacked together in Fig. 1(i). The dashed rectangular frame encloses the stage where each spin-orbit splitting peak, Ge $3d_{3/2}$ and $3d_{5/2}$, becomes broader to infer the coexistence of alloy and germanene component [7]. In other words, the dealloying process occurs in the deposition period from 30 to 40 min, the so-called transition stage. We integrate the intensities of QP single scattering spots as enclosed by the red circle, and Ag(111)-$\sqrt{3} \times \sqrt{3}R30^\circ$ spot clusters at $(\frac{1}{3}\ \frac{1}{3})$ positions as enclosed by the blue circle with increasing deposition time. As shown in Fig. 1(j), while the former increases in a linear manner through the transition stage enclosed by the dashed frame, the latter decreases rapidly from 25 to 30 min and then obviously more slowly in the transition stage from 30 to 40 min. A plausible explanation is that within this stage, striped Ag_2Ge alloy is dealloyed to SP germanene with the same stripe lattice, which serves as the precursor for the formation of QP. If the 50 min deposition time corresponds to 1 ML germanene, then SP germanene with the surface density of 0.74 ML falls in the 35–40 min period, where LEED intensities at the $(\frac{1}{3}\ \frac{1}{3})$ positions plateau.

Figure 2 summarizes the structural information for the SP phase obtained from modeling and fits to LEED and STM data. In Figs. 2(a)–2(c), an example of the LEED data is shown side by side with a simulation based on Ag(111) and the three aligned domains of SP. The Ag(111)-$\sqrt{3} \times \sqrt{3}R30^\circ$ model with the AC direction compressed by 6% ($11a_{\mathrm{AC}} = 31a_{\mathrm{Ag(111)}}$) fits all observed spots for both Ag(111) and SP equally well (see Fig. S2 of the Supplemental Material for details [25]). Magnified examples of the details are included in Fig. 2(c). The STM topography image shown in Fig. 2(d) reveals the three rotational domains of the SP germanene. Figure 2(e) illustrates the spatial relation among the three domains of stripe orientations, and defines the photoemission scanning directions, $\bar{\Gamma}\bar{M}_{\mathrm{Ag(111)}}$ and $\bar{\Gamma}\bar{K}_{\mathrm{Ag(111)}}$, parallel and perpendicular to the one of the stripe domains. The atomic-resolved STM image in the top of Fig. 2(f) shows both SP's honeycomb atomic structure and periodic stripes due to its mismatch with the underlying Ag(111) surface. The brighter regions indicate

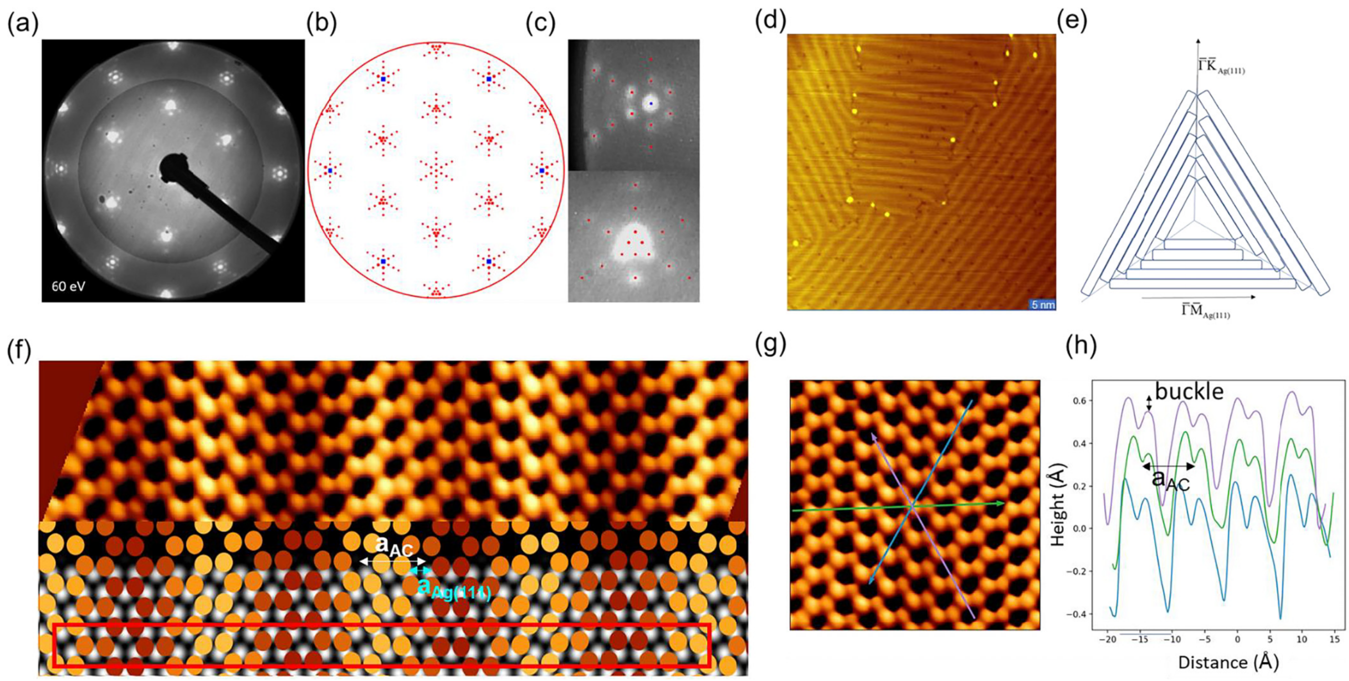

FIG. 2. (a) Measured LEED pattern of SP germanene on Ag(111) at 60 eV. (b) Simulation of (a) based on the $(31 \times \sqrt{3})$ $a_{\mathrm{Ag}(111)}$ unit cell. (c) Magnified LEED patterns with simulation spots superimposed. (d) STM topography ($I_{\mathrm{tunneling}} = 0.78$ nA, $V_{\mathrm{tunneling}} = -0.62$ V) of large-range SP germanene on Ag(111). (e) Schematic illustration of the three domains of SP germanene and the definition of the photoemission symmetry direction with respect to one of the stripe domains. (f) Atomic-resolved STM topography ($I_{\mathrm{tunneling}} = 0.96$ nA, $V_{\mathrm{tunneling}} = -0.0073$ V) of the SP germanene honeycomb on Ag(111) at the top and the corresponding simulation using FK relaxation at the bottom. (g) Data from the same STM scan shown in (f) but with a low-frequency stripe pattern subtracted. (h) Height profiles from line scans in three symmetry directions, extracted from (g).

the stripes on the bridge sites of Ag(111) while the darker regions between the stripes are on the hollow sites. The origin of the topological stripes and their period can be easily explained phenomenologically with a simple 2D Frenkel-Kontorova (FK) relaxation of a honeycomb net of atoms on a hexagonally periodic surface potential, with a fixed higher-order-coincident (HOC) unit cell of $(31 \times \sqrt{3})$ $a_{\mathrm{Ag}(111)}$, as marked by the red rectangular frame. A Hooke's law bond energy $u_{ij} = -f(|\boldsymbol{x}_i - \boldsymbol{x}_j| - a_0)^2$ is defined by magnitude f and equilibrium distance a_0, and the threefold-sinusoidal surface potential is the normalized sum of three plane waves at 0° and ±120°. A full row of 44 atoms is modeled, and the relaxation naturally converges to a simpler centered-rectangular arrangement with its associated symmetries. Results are quite insensitive to the values chosen so long as a_0 does not exceed the average unrelaxed interatomic distance, which is easily satisfied since this upper limit is roughly 20% longer than that for freestanding germanene (see the Frenkel-Kontorova model section of the Supplemental Material for details [25]). For simplicity we chose to use the unrelaxed distance for the illustration in the figure. The relaxation result is shown in the bottom of Fig. 2(f). The color of the individual atom represents its final surface potential, which represents proximity to a top site of the Ag(111) atomic lattice, and is taken as a proxy for final height; i.e., atoms resting in the centers of hollow sites presumably end up lower topographically than those at bridge sites. As shown in Fig. 2(f), the result agrees with the STM image very well, not just the lateral displacements but also the height variation. It is important to point out that while molecular dynamics with optimized force fields and first-principles calculations can be used to quantitatively address the energies involved, results of a simple ball-and-spring implementation of the nearly century-old FK model closely reproduce atomic positions from STM in all three dimensions very faithfully. The only feature of the STM image that could not be reproduced by this model is the pronounced honeycomb buckling, clearly visible in Figs. 2(g) and 2(h), where the STM image of the SP honeycomb has had a long-period wave (4 cycles/HOC unit cell) subtracted, making the remaining atomic buckling more prominent. This up/down buckling pattern is coherent across the entire 80×80 Å STM image. According to the three profiles extracted from three directions in Fig. 2(g), the buckle height is about 0.08 Å with the period of a_{AC}. In Fig. S3 of the Supplemental Material [25], we adopt the x, y, z coordinates of 12 even-numbered rows of honeycomb atoms from the STM data, a single row from the FK relaxation of SP germanene, and the DFT solution provided by Zhang *et al.* [29] based on the honeycomblike Ag atoms in Ag_2Ge alloy for the scatter plot of y and z as a function of x. It indicates that both theoretical approximations, FK and DFT, result in configurations similar to the measured data except for the buckling. It is this buckling that causes height z as a function of x in the STM image to be less sinusoidal as shown in Fig. S3(b). The buckling already strongly suggests the germanene nature. It is also important to note that both theoretical approximation models based on germanene and alloy give rise to the same diffraction pattern shown in Fig. 2(a) because of the common stripe-lattice structure of $(31 \times \sqrt{3})$

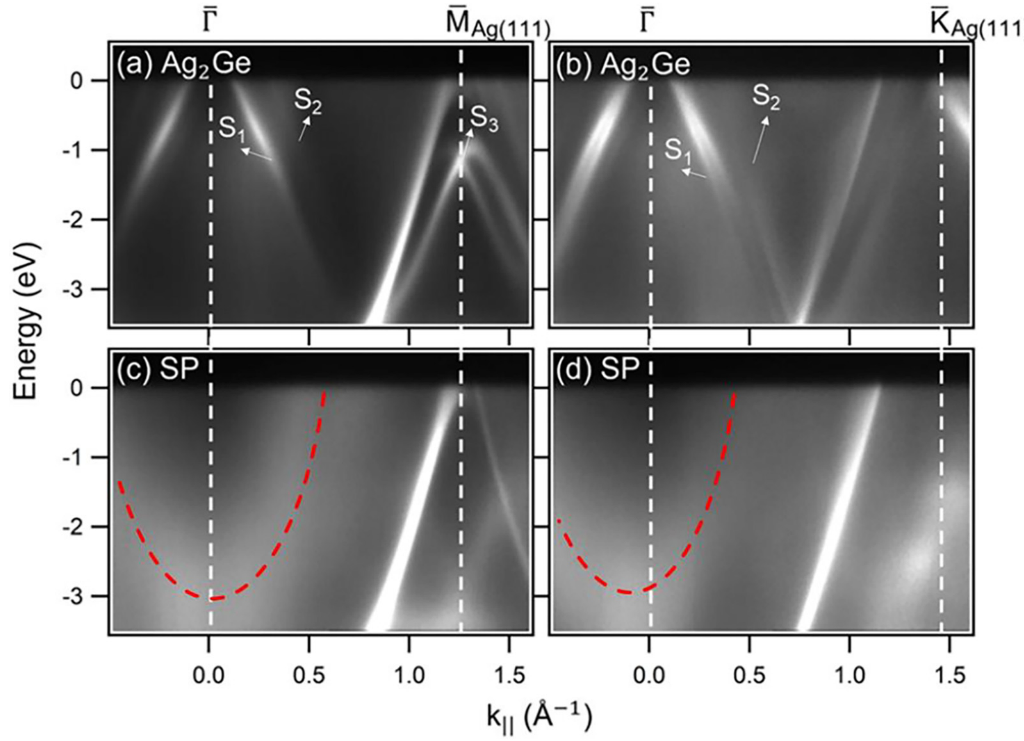

FIG. 3. Measured energy band structures of (a), (b) Ag_2Ge surface alloy and (c), (d) SP germanene in two symmetry directions, $\bar{\Gamma}\bar{M}_{Ag(111)} = 1.256$ $Å^{-1}$ and $\bar{\Gamma}\bar{K}_{Ag(111)} = 1.45$ $Å^{-1}$. The red dashed lines mark the broad and diffused energy bands dispersing about the surface zone center.

$a_{Ag(111)}$. Therefore, to gain deeper insight, measurement of the electronic structures is indispensable.

Figure 3 shows the measured energy band dispersions of Ag_2Ge surface alloy and SP germanene on Ag(111) in two symmetry directions, $\bar{\Gamma}\bar{M}_{Ag(111)}$ and $\bar{\Gamma}\bar{K}_{Ag(111)}$, respectively. One can clearly see the distinct electronic structures between the two. For the former, there are two downward surface-state bands, S_1 and S_2, centered at the surface zone center $\bar{\Gamma}$, and a splitlike surface-state band S_3 centered at the surface zone boundary $\bar{M}_{Ag(111)}$. The three surface-state bands have been investigated in detail previously [36–39]. For the latter, there is a broad and diffused energy band dispersing around $\bar{\Gamma}$. Centered at the surface zone boundary $\bar{M}_{Ag(111)}$ is a V-shaped band with steep dispersion at −3 eV within the bulk Ag band gap projected to the (111) surface. Lin *at al.* [5] indicated that this band was actually an interface-state band between SP germanene and Ag(111) according to first-principles calculation. The broad energy band around $\bar{\Gamma}$ seems pertinent to the direct transition of bulk Ag states; however it does not emerge for Ag_2Ge surface alloy on Ag(111). Upon a close examination, the dispersion appears asymmetric with respect to $\bar{\Gamma}$, especially in the $\bar{\Gamma}\bar{K}_{Ag(111)}$ direction, which should be completely symmetric in light of the fcc bulk Brillouin zone.

Figures 4(a)–4(d) elucidate the step-by-step evolution from the Ag_2Ge surface alloy to SP germanene by checking the energy band structure centered at $\bar{M}_{Ag(111)}$. As shown, the splitlike S_3 band characterizing the Ag_2Ge surface alloy decays in intensity as the Ge coverage increases from 1/3 ML, while the V-shaped band emerges and increases in intensity until the full coverage for SP germanene (0.74 ML) is reached. Figure 4(g) shows the dependence of the energy distribution curve (EDC) at $\bar{M}_{Ag(111)}$ on Ge coverage. Peaks *A*, *B*, and *C* denote the bottom of the V-shaped band for SP germanene, the crossing point of the splitlike S_3 band for the Ag_2Ge surface alloy, and the top of the Ag bulk band edge, respectively. The evolution of peak intensities for *A* and *B* further manifests the behavior depicted in Figs. 4(a)–4(d). For peak *C*, the intensity gradually goes lower with the increasing Ge coverage, indicating the covering of the Ag(111) substrate surface by SP germanene. Figure 4(f) exhibits the corresponding change of the Ge 3*d* core-level peak. As is evident, there is an abrupt energy shift, ~ -0.25 eV, from Ag_2Ge to SP, inferring a dealloying process [7]. The double-peak line shape of each spin-orbit splitting component in the blue curve exhibits the coexistence of Ag_2Ge and SP, corresponding well to the peaks *B* and *A* in Fig. 4(g). It is important to note that a similar process also occurs for Bi atoms deposited on Ag(111); the Ag_2Bi surface alloy completing at 1/3 ML of Bi begins dealloying to the $(p \times \sqrt{3})$ overlayer with increasing Bi [40]. The length of the lattice vector in the Ag(11$\bar{2}$) direction ($\bar{\Gamma}\bar{M}_{Ag(111)}$) is $\sqrt{3}a_{Ag(111)}$, exactly the same as that of SP in the stripe direction. Bi/Ag(111)-$(p \times \sqrt{3})$ finally relaxes to a Bi(110) layer at about 1 ML, similar to SP relaxation to QP germanene. Figures 4(d) and 4(e) show the measured energy band structures of SP in the $\bar{\Gamma}\bar{M}_{Ag(111)}$ and $\bar{\Gamma}\bar{K}_{Ag(111)}$ directions within the bulk Ag projected band gap near the surface zone boundaries, $\bar{M}_{Ag(111)}$ and $\bar{K}_{Ag(111)}$. Figures 4(h) and 4(i) show the calculation counterparts adopting the approximate lattice ratio of $3a_{AC} = 8a_{Ag(111)}$ [5] (see Fig. S4 of the Supplemental Material [25] for the calculated energy band structures in all symmetry directions of Ag(111)). The match between the measurement and calculation is qualitatively agreeable. Comparing the V-shaped feature centered at $\bar{M}_{Ag(111)}$ of both, the calculated one is about 0.9 eV higher,

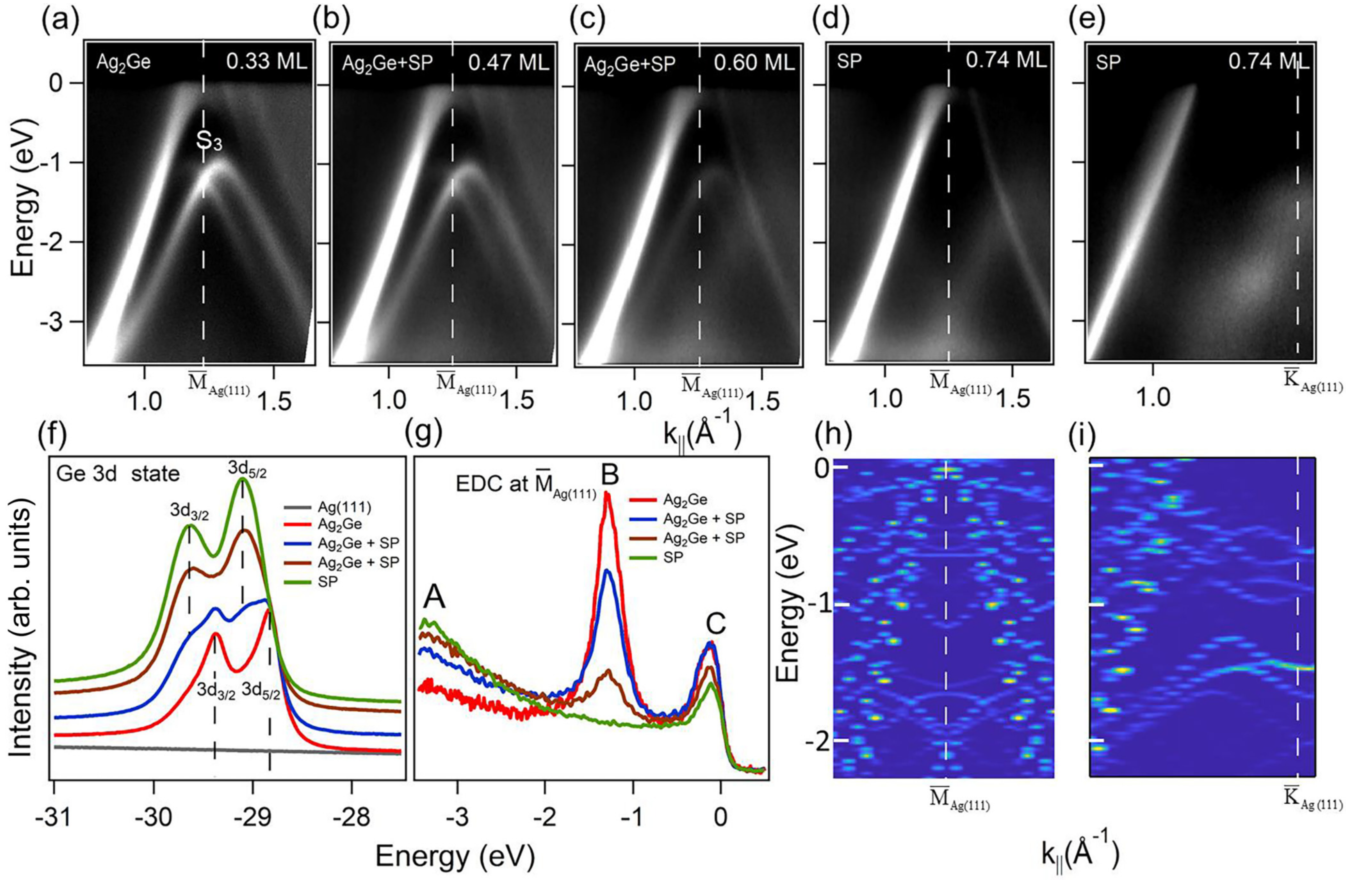

FIG. 4. (a)–(d) Step-by-step evolution of the measured energy band structure near $\bar{M}_{Ag(111)}$ in the $\bar{\Gamma}\bar{M}_{Ag(111)}$ direction for transition from Ag_2Ge surface alloy to SP germanene on Ag(111). (e) The measured energy band structure of SP germanene on Ag(111) near $\bar{K}_{\mathrm{Ag}(111)}$ in the $\bar{\Gamma}\bar{K}_{Ag(111)}$ direction. (f) Step-by-step evolution of the measured Ge 3d core-level peak for transition from Ag_2Ge surface alloy to SP germanene on Ag(111). The spectra are taken at 80 eV. (g) Step-by-step evolution of the measured EDCs at $\bar{M}_{Ag(111)}$ for transition from Ag_2Ge surface alloy to SP germanene. (h), (i) The calculated energy band structures of SP germanene on Ag(111) in the two symmetry directions corresponding to (d), (e).

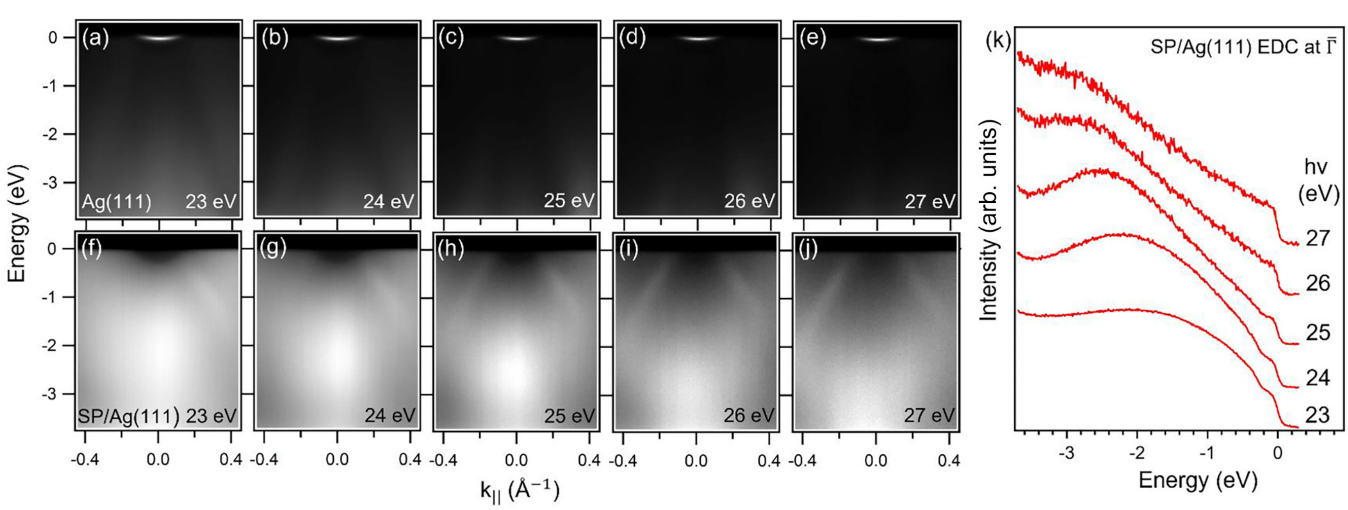

FIG. 5. Photon energy dependence of the measured energy band structures centered at the surface zone center for (a)–(e) Ag(111) and (f)–(j) SP germanene on Ag(111). (k) Photon energy dependence of the measured EDCs from (f)–(j) at the surface zone center.

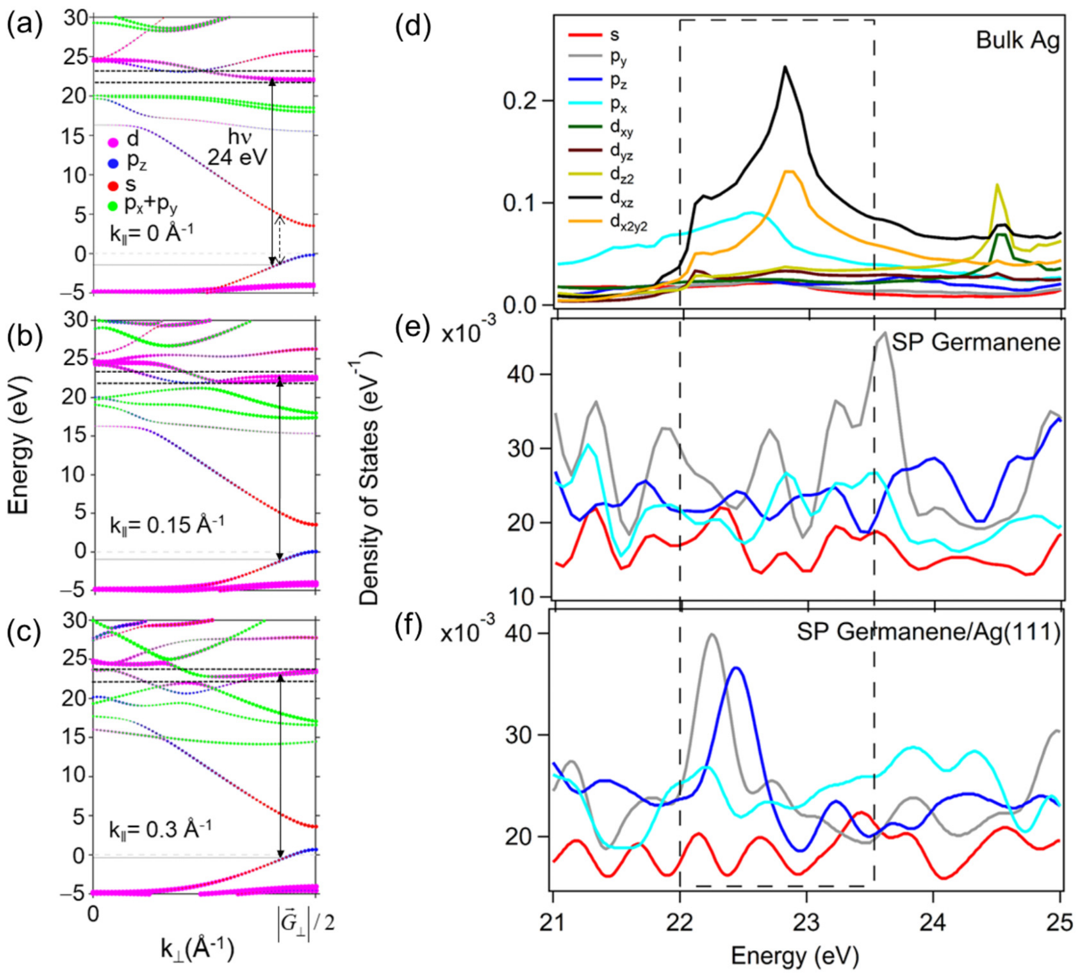

FIG. 6. Calculated bulk Ag energy bands perpendicular to the (111) surface at (a) $k_\parallel = 0$ Å^{-1}, (b) $k_\parallel = 0.15$ Å^{-1}, and (c) $k_\parallel = 0.3$ Å^{-1} in the $\bar{\Gamma}\bar{K}_{Ag(111)}$ direction. The calculated energy-dependent density of states for (d) bulk Ag, (e) freestanding SP germanene, and (f) SP germanene on Ag(111).

and is less dispersed and steep. The calculation shows that the orbital composition of the V-shaped band at $\bar{M}_{\mathrm{Ag}(111)}$ is about 50% from Ag and Ge each, reflecting the strong electronic hybridization between SP germanene and Ag(111) [5]. There are no other electronic features discovered related to the lateral quantum confinement effect as in graphene nanoribbon [41]. It is because unlike graphene nanoribbons, SP germanene does not have definite lateral width except for the domain boundaries separating three different domains of SP germanene, as shown in Fig. 2(d), and the substantial interaction between SP germanene and Ag as indicated from the V-shaped interfacial-state band can smear out the confinement effect. It is likely that before the coverage increases to the full coverage of 0.74 ML for SP germanene, the stripe structure has been established, but mixed with alloys and germanene in different domains.

As mentioned in the previous paragraph, the broad and diffusive bulklike energy band appears simultaneously with the formation of SP germanene. However, it has no counterpart in the calculated electronic structure of SP (see Fig. S4 of the Supplemental Material [25]). Figures 5(a)–5(e) exhibit the measured energy band structures of clean Ag(111) in the $\bar{\Gamma}\bar{K}_{\mathrm{Ag}(111)}$ direction at photon energies from 23 to 27 eV. Figures 5(f)–5(j) exhibit the corresponding measurements for SP germanene. The EDCs at $\bar{\Gamma}$ extracted from Figs. 5(f)–5(j) are stacked in Fig. 5(k) for direct comparison. It is evident that the anomalous broad band shifts away from the Fermi level from ~ -1.5 to ~ -2.5 eV with increasing photon energies, revealing that it originates from a direct transition in $k_\perp$. Note that the faint S_1 surface-state band of $AgGe_2$ residue, which does not shift in energy, serves as a contrast. However such a direct-transition band is completely absent for Ag(111), which only shows a sharp Ag(111) surface-state band near the Fermi level. It is likely that SP germanene on top of Ag(111) strongly modulates the final-state effect for direct transition. This has been previously observed from the adsorption of organic molecules on metal surfaces [42–44]. The peak line shapes of all EDCs in Fig. 5(k) are very broad, whereas those at the photon energies of 24 and 25 eV are more pronounced, implying that direct transition from initial to final bulk Ag states excited at these two photon energies is more efficient.

Figures 6(a)–6(c) show the calculated Ag bulk bands, E versus $k_\perp$, projected to the (111) surface at $k_\parallel$ positions of 0, 0.15, and 0.3 Å^{-1}, respectively, in the $\bar{\Gamma}\bar{K}_{\mathrm{Ag}(111)}$ direction. The calculated Ag bulk bands along $k_\perp$ are folded by $\frac{1}{2}\vec{G}_\perp$ so that the direct transition between the initial and final states can be easily realized. The main orbital composition of each bulk band is denoted by various colors. As one can see, to fulfill the observed direct transitions in Fig. 5, the final-state band has to be the unoccupied one (denoted by pink) with dominant d character at an energy of about 22–23 eV above the Fermi level via the simple relation $E_f - E_i = h\nu$. The matrix element for the photoemission transition rate (or intensity) can be written as $M_{fi} = \langle \psi_f | \vec{A} \cdot \vec{p} | \psi_i \rangle$, where $\vec{A}$ is the vector potential and $\vec{p}$ is the momentum of the electron state. The symmetry of the initial state ψ_i with respect to the photoemission-mirror plane can be even or odd. Our probing beam is p polarized so $\vec{A} \cdot \vec{p}$ is even with respect to the mirror plane. If the electronic state is 2D, the final-state ψ_f is considered as a plane wave for the photoelectron, which has to be even with respect to the mirror plane. However, for a three-dimensional electronic state undergoing the photoemission process, the final-state ψ_f is subject to the bulk crystal and possesses the orbital character of the unoccupied final band. For the present direct-transition case, the initial states of bulk Ag are the s and p_z type (denoted by red and blue). Normally, the transition would go to the unoccupied band with the same s and p_z type, as is indicated by the dashed arrow in Fig. 6(a). Such a direct transition has been widely identified from a clean bulk Ag(111) surface [45]. When SP germanene forms on top of Ag(111), the transition changes to the unoccupied band with dominant d orbitals, as indicated by the solid arrows in Figs. 6(a)–6(c). In light of the transition matrix element, this is unfavorable unless the unoccupied final-state band takes on substantial s and p_z character. Germanene, like graphene, consists of covalent bonding between composite atoms. The π bonds that stick out of the honeycomb planes are very likely to interact with the underlying substrate atoms, namely, the hybridization between π bands of germanene and the bulk bands of Ag. As a result of such interaction, the wave functions of the Ag bulk states near the SP germanene/Ag(111) interface can possess more pronounced p_z character. In order to confirm this, we calculated the density of states (DOS) for bulk Ag projected to the (111) surface, freestanding SP germanene, and SP germanene on Ag(111), as shown in Figs. 6(d)–6(f), in the energy range between 21 and 25 eV above the Fermi level. For bulk Ag, in the energy window (22–23.5 eV) enclosed by the dashed frame, one can see the d_{xz} orbital dominates the DOS in Fig. 6(d). This energy window is also expressed in Figs. 6(a)–6(c) by the dashed frame enclosing parts of the d bands denoted by pink. In this energy window of Fig. 6(e), the p_y orbital dominates for the valence electrons of freestanding SP. Figure 6(f) shows that the p_z orbital of SP germanene is substantially enhanced on Ag(111), inferring the hybridization between the SP germanene π band and the Ag d band in the unoccupied level. The direct transitions indicated by the solid arrows in Figs. 6(a)–6(c) become understandable because Ag d bands near SP germanene/Ag(111) interface convolute with the p_z orbital. It is noteworthy that the change of Ag occupied d-band states ranging from −4 to −8 eV due to the adsorption of organic molecules with π bonds was commonly observed [43]. Strong hybridization can smear out π orbitals, making germanene more sp^2- and metal-like as revealed by Kesper *et al.* [4] from their structure determination. Figures 6(a)–6(c) illustrate how the initial energy of this direct transition disperses upward toward the Fermi level with increasing $k_\parallel$ in $\bar{\Gamma}\bar{K}_{\mathrm{Ag}(111)}$ for a photon energy of 24 eV; however, extra care needs to be taken when simulating the measured energy dispersions in Figs. 5(f)–5(j). The final-state effect mostly refers to the umklapp scattering with the extra reciprocal vector imposed from the adlayer such that $\vec{k}_{f\parallel} = \vec{k}_{i\parallel} + \vec{G}_s + \vec{G}_{\mathrm{adlayer}}$ [43,44]. In the present case, $\vec{G}_s$ and $\vec{G}_{\mathrm{adlayer}}$ are those of the Ag(111) surface and SP germanene. Since we only focus on the energy band structures within the first Brillouin zone of Ag(111), $\vec{G}_s = 0$. Marchenko *et al.* [44] successfully reproduced the measured anomalous band at the surface zone center for C_{60}/Cu(111) by backfolding of the Cu bulk band edge around the zone boundary $\bar{M}$ via the $\vec{G}_{\mathrm{adlayer}}$ of the (4 × 4) superstructure of C_{60}. However, as shown in Fig. S6 of the Supplemental Material [25], this scenario does not apply to SP germanene/Ag(111), and SP germanene, except for the stripe direction, is incommensurate with the Ag(111) substrate so we only consider the umklapp effect corresponding to the HOC period. As shown in Figs. 2(d) and 2(f), SP germanene forms as a uniform array that renders a long-range order in the AC direction with the HOC period $11a_{\mathrm{AC}} = 31a_{\mathrm{Ag}(111)}$. The corresponding HOC reciprocal vector is 0.078 Å^{-1}. Electronic-structure modulation induced by the moiré-umklapp-scattering effect has often been observed in 2D materials, which have lattice mismatches with the underlying substrates, e.g., graphene/Ir(111) [46,47]. By the same token, we applied such umklapp-scattering effect in simulating the measured direct-transition bands in Fig. 5 just by offsetting the $k_\parallel$ values, e.g., 0, 0.15, and 0.3 Å^{-1} in Figs. 6(a)–6(c), by $\pm|\vec{G}_{\mathrm{HOC}}|$ for the initial-state band that fits the direct transition. Note that the effective HOC period changes with the direction relative to the AC direction, so a general expression for the HOC reciprocal vector is $|\vec{G}_{\mathrm{HOC}}| = \frac{2\pi}{|\vec{a}_{\mathrm{HOC}}|\cos 26.88^\circ}$. $|\vec{a}_{\mathrm{HOC}}| = 31a_{\mathrm{Ag}(111)}\sec\theta$, where θ is the angle between the AC direction and that of HOC (see Figs. S2 and S5 of the Supplemental Material for details [25]). Referring to Fig. 2(e), the $\bar{\Gamma}\bar{K}_{\mathrm{Ag}(111)}$ ($\bar{\Gamma}\bar{M}_{\mathrm{Ag}(111)}$) direction passes the bottom domain of SP with $\theta = 0^\circ$ ($\theta = 90^\circ$) and another two top domains with $\theta = 60^\circ$ ($\theta = 30^\circ$). It is noteworthy that along the $\bar{\Gamma}\bar{M}_{\mathrm{Ag}(111)}$ direction, the inversion symmetry between positive and negative k momentum is maintained in light of the stripe orientations of the three domains; however, such symmetry is broken in the $\bar{\Gamma}\bar{K}_{\mathrm{Ag}(111)}$ direction. Therefore, the observed lower symmetry of the direct-transition band in $\bar{\Gamma}\bar{K}_{\mathrm{Ag}(111)}$ in Fig. 3(d) can be understood. $|\vec{G}_{\mathrm{HOC}}| = 0.078$ Å^{-1} corresponding to $\theta = 0^\circ$ is used for the measured bulklike band in the $\bar{\Gamma}\bar{K}_{\mathrm{Ag}(111)}$ direction, and $|\vec{G}_{\mathrm{HOC}}| = 0.068$ Å^{-1} corresponding to $\theta = 30^\circ$ is used for the measured one in the $\bar{\Gamma}\bar{M}_{\mathrm{Ag}(111)}$ direction. The umklapp-scattering effect is applied in the bottom SP domain (neglecting that from the top two domains for simplicity) in the former, and in the top two SP domains (neglecting that from the bottom domain due to being commensurate) in the latter. The simulation results, sampling more $k_\parallel$ points than the three values illustrated in Figs. 6(a)–6(c), are superimposed onto the measured direct-transition bands taken at the photon energies of 24 and 25 eV in both symmetry directions, as shown in Fig. 7. The match is reasonable. It is noteworthy that as $k_\parallel$ increases, the final-state d band

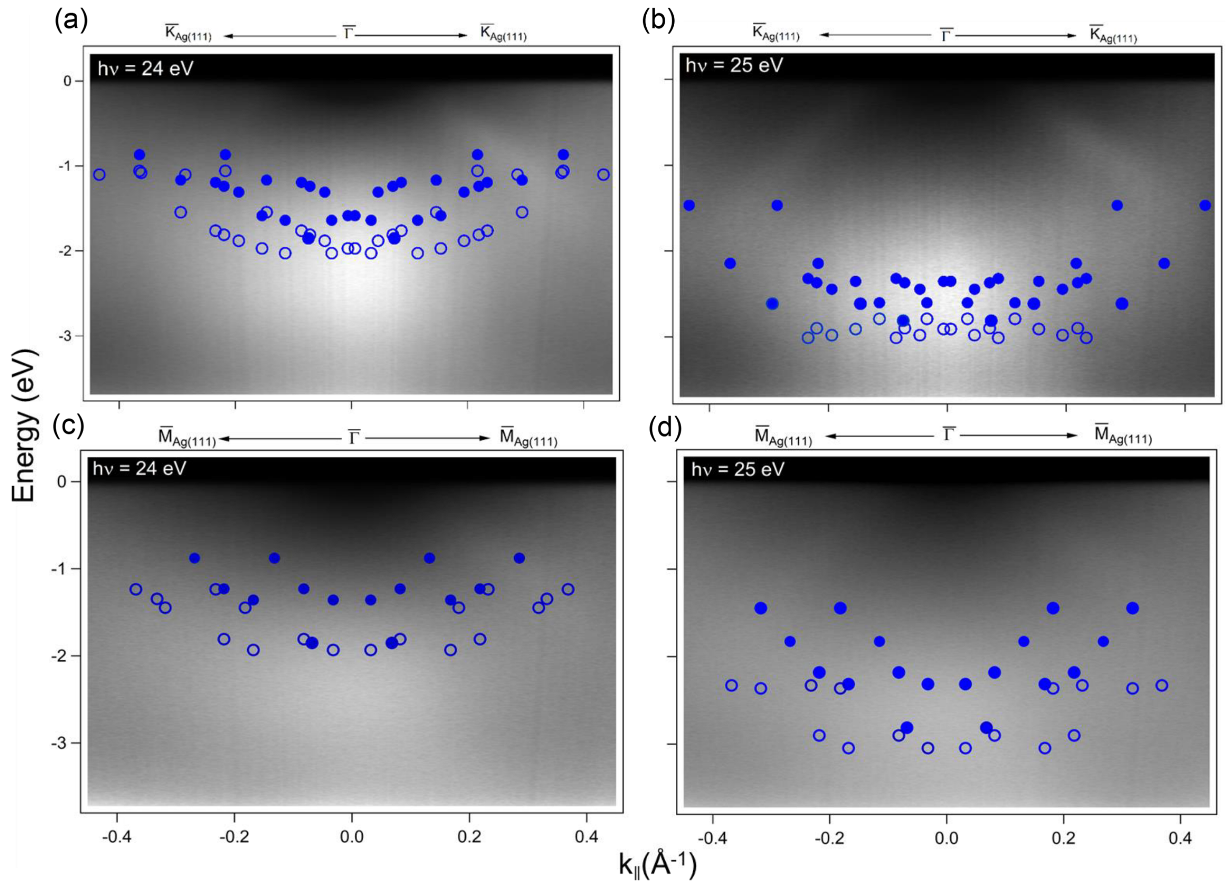

FIG. 7. Measured energy band structures of SP germanene on Ag(111) and the simulated counterpart in the $\bar{\Gamma}\bar{K}_{Ag(111)}$ direction at the photon energy of (a) 24 and (b) 25 eV, and in the $\bar{\Gamma}\bar{M}_{Ag(111)}$ direction at the photon energy of (c) 24 and (d) 25 eV.

separates to two branches as seen in Figs. 6(b) and 6(c), causing the measured direct-transition band to be more diffusively broadened. The filled and hollow circles indicate the transitions to two different final-state branches. In short, we have demonstrated a method to judge the intrinsic identity as a 2D overlayer or an alloy layer by probing the final-state effect on the bulk electronic structures of an underlying substrate.

IV. CONCLUSION

Using a model of relaxed 2D honeycomb germanene with a $(31 \times \sqrt{3})$ $a_{\mathrm{Ag}(111)}$ HOC period on a hexagonal (threefold sinusoidal) surface potential for the Ag(111) surface, we reproduce the STM atomic configuration for SP germanene on Ag(111). This lattice structure perfectly fits LEED spots of SP germanene. From the perspective of electronic structures, the step-by-step evolution from the S_3 surface state of Ag_2Ge to the V-shaped interface-state band characterizing SP germanene at the surface zone boundary $\bar{M}_{\mathrm{Ag}(111)}$ with increasing Ge coverage was carefully examined. The corresponding Ge 3d core-level state also exhibits the consistent behavior. Finally, the anomalous bulklike broad band emerging upon the formation of SP germanene was demonstrated to derive from the direct-transition photoemission from the bulk Ag occupied sp band to the unoccupied d bands, which survives the symmetry-selection rule due to the strong hybridization between the π bonds of SP germanene and the d electrons of bulk Ag near the SP germanene/Ag(111) interface. The existence of SP germanene is therefore further confirmed. The transition from Ag_2Ge alloy to QP germanene on Ag(111) goes through not only a chemical decoupling, but a subsequent balancing between tensile and interfacial strain. During the balancing process, Ag_2Ge alloy and SP germanene can coexist in the common stripe configuration. The former diminishes while the latter grows with the increasing Ge coverage to reach a continuous transition and final relaxation to QP germanene. Our results indicate that Ag(111) provides an excellent platform for growth of germanene that accommodates various forms under different conditions because of its covalent-bond nature, providing deep insight into the subtle growing mechanism of a tetrahedrally bonded Xene on an incommensurate substrate.

ACKNOWLEDGMENTS

This research was supported by the National Science and Technology Council (Grants No. NSTC 111-2112-M-007-031 and No. 112-2112-M-007-047 for S.-J.T, Grant No. NSC 110-2112-M-002-040-MY3 for W.W.P., and Grant No. NSTC 112-2112-M-007-034-MY3 for H.-T.J.). W.W.P. acknowledges support from the Center for Quantum Science and Technology (CQST) and the Center of Atomic Initiative for New Materials (AI-MAT) within the framework of the Higher Education Sprout Project by the Ministry of Education (MOE) in Taiwan. H.-T.J. acknowledges NCHC, CINC-NTU, and AS-iMATE-111-12, Taiwan, for technical support.

[1] A. Molle, J. Goldberger, M. Houssa, Y. Xu, S. C. Zhang, and D. Akinwande, Buckled two-dimensional Xene sheets, Nat. Mater. **16**, 163 (2017).

[2] P. Vogt, P. De Padova, C. Quaresima, J. Avila, E. Frantzeskakis, M. C. Asensio, A. Resta, B. Ealet, and G. Le Lay, Silicene: Compelling experimental evidence for graphene-like two-dimensional silicon, Phys. Rev. Lett. **108**, 155501 (2012).

[3] A. Molle, C. Grazianetti, L. Tao, D. Taneja, Md. H. Alam, and D. Akinwande, Silicene, silicene derivatives, and their device applications, Chem. Soc. Rev. **47**, 6370 (2018).

[4] L. Kesper, J. A. Hochhaus, M. Schmitz, M. G. H. Schulte, U. Berges, and C. Westphal, Tracing the structural evolution of quasi-freestanding germanene on Ag(111), Sci. Rep. **12**, 7559 (2022).

[5] C.-H. Lin, A. Huang, W. W. Pai, W.-C. Chen, T.-Y. Chen, T.-R. Chang, R. Yukawa, C.-M. Cheng, C.-Y. Mou, I. Matsuda, T.-C. Chiang, H.-T. Jeng, and S.-J. Tang, Single-layer dual germanene phases on Ag(111), Phys. Rev. Mater. **2**, 024003 (2018).

[6] J. Yuhara, H. Shimazu, K. Ito, A. Ohta, M. Araidai, M. Kurosawa, M. Nakatake, and G. Le Lay, Germanene epitaxial growth by segregation through Ag(111) thin films on Ge(111), ACS Nano **12**, 11632 (2018).

[7] T.-Y. Chen, D. Mikolas, S. Chiniwar, A. Huang, C.-H. Lin, C.-M. Cheng, C.-Y. Mou, H.-T. Jeng, W. W. Pai, and S.-J. Tang, Germanene structure enhancement by adjacent insoluble domains of lead, Phys. Rev. Res. **3**, 033138 (2021).

[8] J. Yuhara, Y. Fujii, K. Nishino, N. Isobe, M. Nakatake, L. Xian, A. Rubio, and G. Le Lay, Large area planar stanene epitaxially grown on Ag(111), 2D Mater. **5**, 025002 (2018).

[9] F.-F. Zhu, W.-J. Chen, Y. Xu, C. -L. Gao, D.-D. Guan, C.-H. Liu, D. Qian, S.-C. Zhang, and J.-F. Jia, Epitaxial growth of two-dimensional stanene, Nat. Mater. **14**, 1020 (2015).

[10] J. Yuhara, B. He, N. Matsunami, M. Nakatake, and G. Le Lay, Graphene's latest cousin: Plumbene epitaxial growth on a "nano watercube", Adv. Mater. **31**, 1901017 (2019).

[11] W.-H. Chen *et al.*, Enhanced superconductivity and Rashba effect in a buckled plumbene-Au kagome superstructure, Adv. Sci. **10**, 2300845 (2023).

[12] B. Feng, O. Sugino, R-Y. Liu, J. Zhang, R. Yukawa, M. Kawamura, T. Iimori, H. Kim, Y. Hasegawa, H. Li, L. Chen, K. Wu, H. Kumigashira, F. Komori, T.-C. Chiang, S. Meng, and I. Matsuda, Dirac fermions in borophene, Phys. Rev. Lett. **118**, 096401 (2017).

[13] N. T. Cuong, I. Tateishi, M. Cameau, M. Niibe, N. Umezawa, B. Slater, K. Yubuta, T. Kondo, M. Ogata, and S. Okada, Topological Dirac nodal loops in nonsymmorphic hydrogenated monolayer boron, Phys. Rev. B **101**, 195412 (2020).

[14] F. Reis, G. Li, L. Dudy, M. Bauernfeind, S. Glass, W. Hanke, R. Thomale, J. Schäferm, and R. Claessen, Bismuthene on a SiC substrate: A candidate for a high-temperature quantum spin Hall material view, Science **357**, 287 (2017).

[15] V. Kochat, A. Samanta, Y. Zhang, S. Bhowmick, P. Manimunda, S. A. S. Asif, A. S. Stender, R. Vajtai, A. K. Singh, C. S. Tiwary, and P. M. Ajayan, Atomically thin gallium layers from solid-melt exfoliation, Sci. Adv. **4**, e1701373 (2018).

[16] L. Li, Y. Yu, G. J. Ye, Q. Ge, X. Ou, H. Wu, D. Feng, X. H. Chen, and Y. Zhang, Black phosphorus field-effect transistors, Nat. Nanotechnol. **9**, 372 (2014).

[17] S. M. Beladi-Mousavi, A. M. Pourrahimi, Z. Sofer, and M. Pumera, Atomically thin 2D-arsenene by liquid-phased exfoliation: Toward selective vapor sensing, Adv. Funct. Mater. **29**, 1807004 (2018).

[18] X. Wu, Y. Shao, H. Liu, Z. Feng, Y.-L. Wang, J.-T. Sun, C. Liu, J.-O. Wang, Z.-L. Liu, S.-Y. Zhu, Y.-Q. Wang, S.-X. Du, Y.-G. Shi, K. Ibrahim, and H.-J. Gao, Epitaxial growth and air-stability of monolayer antimonene on $PdTe_2$, Adv. Mater. **29**, 1605407 (2017).

[19] J. Qin, G. Qiu, J. Jian, H. Zhou, L. Yang, A. Charnas, D. Y. Zemlyanov, C.-Y. Xu, X. Xu, W. Wu, H. Wang, and P. D. Ye, Controlled growth of a large-size 2D selenium nanosheet and its electronic and optoelectronic applications, ACS Nano **11**, 10222 (2017).

[20] Q. Wang, M. Safdar, K. Xu, M. Mirza, Z. Wang, and J. He, Van der Waals epitaxy and photoresponse of hexagonal tellurium nanoplates on flexible mica sheets, ACS Nano **8**, 7497 (2014).

[21] C. C. Liu, W. Feng, and Y. Yao, Quantum spin Hall effect in silicene and two-dimensional germanium, Phys. Rev. Lett. **107**, 076802 (2011).

[22] M. Derivaz, D. Dentel, R. Stephan, M.-C. Hanf, A. Mehdaoui, P. Sonnet, and C. Pirri, Continuous germanene layer on Al(111), Nano Lett. **15**, 2510 (2015).

[23] P. Bampoulis, L. Zhang, A. Safaei, R. van Gastel, B. Poelsema, and H. J. W. Zandvliet, Germanene termination of Ge_2Pt crystals on Ge(110), J. Phys.: Condens. Matter **26**, 442001 (2014).

[24] L. Zhang, P. Bampoulis, A. N. Rudenko, Q. Yao, A. van Houselt, B. Poelsema, M. I. Katsnelson, and H. J. W. Zandvliet, Structural and electronic properties of germanene on MoS_2, Phys. Rev. Lett. **116**, 256804 (2016).

[25] See Supplemental Material at http://link.aps.org/supplemental/10.1103/PhysRevResearch.6.043190 for extra measured and calculated electronic structures, and more detailed model explanation.

[26] A. J. Mannix, X.-F. Zhou, B Kiraly, J. D. Wood, D. Alducin, B. D. Myers, X. Liu, B. L. Fisher, U. Santiago, J. R. Guest, M. J. Yacaman, A. Ponce, A. R. Oganov, M. C. Hersam, and N. P. Guisinger, Synthesis of borophenes: Anisotropic, two-dimensional boron polymorphs, Science **350**, 1513 (2015).

[27] S. Chahal, A. Bandyopadhyay, C. S. Yang, and P. Kumar, Beryllene, the lightest Xene, npj 2D Mater Appl. **7**, 55 (2023).

[28] K. Zhang, R. Bernard, Y. Borensztein, H. Cruguel, and G. Prévot, Growth of germanium-silver surface alloys followed by *in situ* scanning tunneling microscopy: Absence of germanene formation, Phys. Rev. B **102**, 125418 (2020).

[29] K. Zhang, D. Sciacca, A. Coati, R. Bernard, Y. Borensztein, P. Diener, B. Grandidier, I. Lefebvre, M. Derivaz, C. Pirri, and G. Prévot, Resolving the structure of the striped Ge layer on Ag(111): Ag_2Ge surface alloy with alternate fcc and hcp domains, Phys. Rev. B **104**, 155403 (2021).

[30] *CRC Handbook of Chemistry and Physics*, 93rd ed., edited by W. M. Haynes (CRC Press, Boca Raton, FL, 2012), Sec. 12, pp. 15–18.

[31] G. Kresse and J. Hafner, *Ab initio* molecular dynamics for open-shell transition metals, Phys. Rev. B **48**, 13115 (1993).

[32] G. Kresse and J. Furthmüller, Efficient iterative schemes for *ab initio* total-energy calculations using a plane-wave basis set, Phys. Rev. B **54**, 11169 (1996).

[33] J. P. Perdew, K. Burke, and M. Ernzerhof, Generalized gradient approximation made simple, Phys. Rev. Lett. **77**, 3865 (1996).

[34] P. V. C. Medeiros, S. Stafström, and J. Björk, Effects of extrinsic and intrinsic perturbations on the electronic structure of graphene: Retaining an effective primitive cell band structure by band unfolding, Phys. Rev. B **89**, 041407 (2014).

[35] P. V. C. Medeiros, S. S. Tsirkin, S. Stafström, and J. Björk, Unfolding spinor wave functions and expectation values of general operators: Introducing the unfolding-density operator, Phys. Rev. B **91**, 041116 (2015).

[36] S. Chiniwar, A. Huang, T.-Y. Chen, C.-H. Lin, C.-R. Hsing, W.-C. Chen, C.-M. Cheng, H.-T. Jeng, C. M. Wei, W. W. Pai, and S.-J. Tang, Substrate-mediated umklapp scattering at the incommensurate interface of a monatomic alloy layer, Phys. Rev. B **99**, 155408 (2019).

[37] W. Wang, H. M. Sohail, J. R. Osiecki, and R. I. G. Uhrberg, Broken symmetry induced band splitting in the Ag_2Ge surface alloy on Ag(111), Phys. Rev. B **89**, 125410 (2014).

[38] E. Golias, E. Xenogiannopoulou, D. Tsoutsou, P. Tsipas, S. A. Giamini, and A. Dimoulas, Surface electronic bands of submonolayer Ge on Ag(111), Phys. Rev. B **88**, 075403 (2013).

[39] Y Liu, J. Zhuang, C. Liu, J. Wang, X. Xu, Z. Li, J. Zhong, and Y. Du, Role of atomic interaction in electronic hybridization in two-dimensional Ag_2Ge nanosheets, J. Phys. Chem. C **121**, 16754 (2017).

[40] K. H. L. Zhang, I. M. McLeod, Y. H. Lu, V. R. Dhanak, A. Matilainen, M. Lahti, K. Pussi, R. G. Egdell, X.-S. Wang, A. T. S. Wee, and W. Chen, Observation of a surface alloying-to-dealloying transition during growth of Bi on Ag(111), Phys. Rev. B **83**, 235418 (2011).

[41] H. Karakachian, T. T. Nhung Nguyen, J. Aprojanz, A. A. Zakharov, R. Yakimova, P. Rosenzweig, C. M. Polley, T. Balasubramanian, C. Tegenkamp, S. R. Power, and U. Starke, One-dimensional confinement and width-dependent bandgap formation in epitaxial graphene nanoribbons, Nat. Commun. **11**, 6380 (2020).

[42] F. C. Bocquet, L. Giovanelli, P. Amsalem, L. Petaccia, D. Topwal, S. Gorovikov, M. Abel, N. Koch, L. Porte, A. Goldoni, and J.-M. Themlin, Final-state diffraction effects in angle-resolved photoemission at an organic-metal interface, Phys. Rev. B **84**, 241407 (2011).

[43] L. Giovanelli, F. C. Bocquet, P. Amsalem, H.-L. Lee, M. Abel, S. Clair, M. Koudia, T. Faury, L. Petaccia, and D. Topwal, Interpretation of valence band photoemission spectra at organic-metal interfaces, Phys. Rev. B **87**, 035413 (2013).

[44] D. Marchenko, M. Krivenkov, M. Sajedi, A. Fedorov, O. Rader, and A. Varykhalov, Revisiting the realization of artificial graphene in C_{60}/Cu(111), Phys. Rev. B **108**, 115155 (2023).

[45] T. Miller, W. E. McMahon, and T. C. Chiang, Interference between bulk and surface photoemission transitions in Ag(111), Phys. Rev. Lett. **77**, 1167 (1996).

[46] E. Rotenberg and A. Bostwick, Superlattice effects in graphene on SiC(0001) and Ir(111) probed by ARPES, Synth. Met. **210**, 85 (2015).

[47] P. Sutter, M. Hybertsen, J. Sadowski, and E. Sutter, Electronic structure of few-layer epitaxial graphene on Ru (0001), Nano Lett. **9**, 2654 (2009).